Coastal forecast through coupling of Deep Learning and hydro-morphodynamical modelling

Pavitra Kumar[1] and Nicoletta Leonardi[1]

[1]University of Liverpool

November 24, 2022

Abstract

As climate-driven risks for the world's coastlines increase, understanding and predicting morphological changes as well as developing efficient systems for coastal forecast has become of the foremost importance for adaptation to climate change and informed coastal management choices. Artificial Intelligence, especially deep learning, is a powerful technology that has been rapidly evolving over the last couple of decades and can offer new means of analysis for the coastal science field. Yet, the potential of these technologies for coastal geomorphology remains relatively unexplored with respect to other scientific fields. This article investigates the use of Artificial Neural Networks and Bayesian Networks in combination with fully coupled hydrodynamics and morphological models (Delft3D) for predicting morphological changes and sediment transport along coastal systems. Two sets of deep learning models were tested, one set relying on localized modelling outputs or localized data sources and one set having reduced dependency from modeling outputs and, once trained, solely relying on boundary conditions and coastline geometry. The first set of models provides regression values greater than 0.95 and 0.86 for training and testing. The second set of reduced-dependency models provides regression values greater than 0.84 and 0.76 for training and testing. Both model types require a running time of the order of minutes, compared to the several hours of running times of the hydrodynamic models. Our results highlight the potential of deep learning and statistical models for coastal applications.

Coastal forecast through coupling of Deep Learning and hydro-morphodynamical modelling

Pavitra Kumar[1*] and Nicoletta Leonardi[1]

[1]Department of Geography and Planning, School of Environmental Sciences, University of Liverpool, Chatham Street, Liverpool, L69 7ZT, UK

* Corresponding Author: pavitrakumar27@gmail.com

Abstract:

As climate-driven risks for the world's coastlines increase, understanding and predicting morphological changes as well as developing efficient systems for coastal forecast has become of the foremost importance for adaptation to climate change and informed coastal management choices. Artificial Intelligence, especially deep learning, is a powerful technology that has been rapidly evolving over the last couple of decades and can offer new means of analysis for the coastal science field. Yet, the potential of these technologies for coastal geomorphology remains relatively unexplored with respect to other scientific fields. This article investigates the use of Artificial Neural Networks and Bayesian Networks in combination with fully coupled hydrodynamics and morphological models (Delft3D) for predicting morphological changes and sediment transport along coastal systems. Two sets of deep learning models were tested, one set relying on localized modelling outputs or localized data sources and one set having reduced dependency from modeling outputs and, once trained, solely relying on boundary conditions and coastline geometry. The first set of models provides regression values greater than 0.95 and 0.86 for training and testing. The second set of reduced-dependency models provides regression values greater than 0.84 and 0.76 for training and testing. Both model types require a running time of the order of minutes, compared to the several hours of running times of the hydrodynamic models. Our results highlight the potential of deep learning and statistical models for coastal applications.

Plain language summary:

Predicting future amounts of erosion/sedimentation and sediment transport along a coastline is important for coastline management in response to climate change. Artificial intelligence is a technique which has been widely used to make predictions in variety of engineering fields, but its potential hasn't been fully explored for coastal science. This study proposes different Artificial Intelligence models for prediction of erosion/sedimentation rates and sediment transport along coastlines. These Artificial Intelligence models require some input data which are retrieved from traditional numerical models, commonly used to reproduce the movement of sediments and water. These traditional models require a lot of computer power and time to give results. The Artificial Intelligence models that we propose here can instead provide predictions of coastal change almost instantaneously and with minimal computer power. We tested two types of Artificial Intelligence Models. The first set of models are based on a large amount of input data and gives predictions which are very accurate (around 90%). The second set of models are based on a very limited amount of input data which can be very easy to find for coastal managers. The latter don't work as good as the previous set but still provide information with 70% accuracy.

Keywords: Morphological changes; Sediment Transport; Neural Networks; Bayesian Networks; Delft3D

1. Introduction

More than 600 million people live along coastal areas less than 10 meters above sea level and the ocean economy, and associated ecosystem services are worth around 3 to 6 trillion annually (Deutz, Kellett, & Zoltani, 2018; UNCC, 2020). The unfolding impact of climate change on the coastal zone is expected to be increasingly disruptive at all spatial scales and derives from the complex overlaps of multiple agents including sea level rise, storms, and anthropogenic influences. For instance, in the UK alone, the need to realign coastal defenses in response to sea level rise is expected to increase the cost of coastal infrastructure maintenance by 150-400% (Dawson et al., 2016). Projections from IPCC indicate that Europe will face storms with higher frequency and the sea level rise will increase the risk of storms and tidal floods leading to greater erosion (Huang-Lachmann & Lovett, 2016). In Europe, the Netherlands is expected to be most affect by sea level rise and more than 4 million people will be living below sea level by 2100 (Buchholz, 2020). According to Nunez and Staff (2022), in 2050 the United States is predicted to receive damaging floods 10 times more than it does today. Population living in the East and Gulf Coasts are among the most vulnerable to flooding. Out of the huge number of people affected by the rising sea levels, 70% of the people are estimated to be living in just eight countries in Asia (Buchholz, 2020). Most affected people will be from China followed by Bangladesh and India. People in Vietnam, Indonesia, Thailand, the Philippines, and Japan would also be largely affected.

Coastal change results from the imbalance between the import and export of sediments, with sediment starvation been normally associated to coastal erosion. Coastline mobility takes place over a yearly time scale but high intensity storm events can lead to significant coastal changes (Plant, Robert Thieler, & Passeri, 2016). Understanding and predicting coastlines evolution is essential for climate adaptation and the correct management of coastal systems.

Numerical models have been one of the preferred tools for investigating coastal hydrodynamics and coastal change and underpin a variety of coastal engineering applications (e.g., Ciavola et al. (2011) and USGS (2015); Lyddon et al., 2019; King et al., 2021) with sophisticated modelling suite been able to predict both hydrodynamic and morphological conditions under different scenarios (C. Chen et al., 2022; Muñoz et al., 2022; Shchepetkin & McWilliams, 2005). These numerical models can be computationally expensive and are not always easily available to a variety of stakeholders. Artificial Intelligence applications have been also used for coastal applications. Sumangala and Warrior (2022) combined Artificial Neural Network (ANN) and numerical simulations to improve the prediction of current velocities in the near-shelf and far-shelf regions of northern bay of Bengal. Rodriguez-Delgado, Bergillos, and Iglesias (2019) utilized ANN for optimization of layout and position of a wave farm for coastal protection at Playa Granada, a beach on Mediterranean coast of southern Spain. López, Aragonés, Villacampa, and Compañ (2018) predicted the cross-shore beach profile using ANN for the sand beaches of coast of province of Valencia, Spain.

However, there are still many unknown about the potential of combining Artificial Intelligence techniques with hydro-morphodynamic modelling and this manuscript aims at investigating synergies between the two methodologies and their potential for predicting morphological changes and sediment transport along the coastline. The main goal of this manuscript is the development of a procedure allowing maximization of numerical modelling outputs for a variety of coastal application through their embedding within computationally efficient data-driven models.

Within this context, two sets of Artificial Intelligence models, aimed at predicting coastal change and suspended sediment transport, were tested in combination with hydro-morphodynamic modelling. One set relying on localized modelling outputs or localized data sources and one set having a reduced dependency from modelling outputs and, once trained, solely relying on boundary conditions information.

Specifically, a hydro-morphodynamic model was developed for Morecambe Bay, UK using Delft3D and was combined that with 4 different Artificial Neural Networks and two

Bayesian Networks models with the goal of forecasting Sediment transport and morphological changes along the coastline.

The test case in analysis is Morecambe Bay, a macrotidal embayment located in the north-west of England. Morecambe Bay (fig. 1) opens south-west into the Irish sea and most of its shoreline is covered in fine sand (Mason, Scott, & Dance, 2010). Intertidal zones are very susceptible to changes mainly in sandbanks and subtidal channels, which can be noticed even within a single season. Morecambe Bay experiences spring tidal waves with amplitudes up to 10m. The fetch length of waves for Morecambe Bay is constrained by landmasses such as Ireland and Isle of Man and sprints at bay mouth. However, the significant wave height at the mouth of the bay reaches up to 2m for about 10% of the year and for the remaining duration of the year significant wave height remain around 0.5m. Coastal change and suspended sediment transport in Morecambe Bay were simulated under different external forcing conditions using Delft3D.

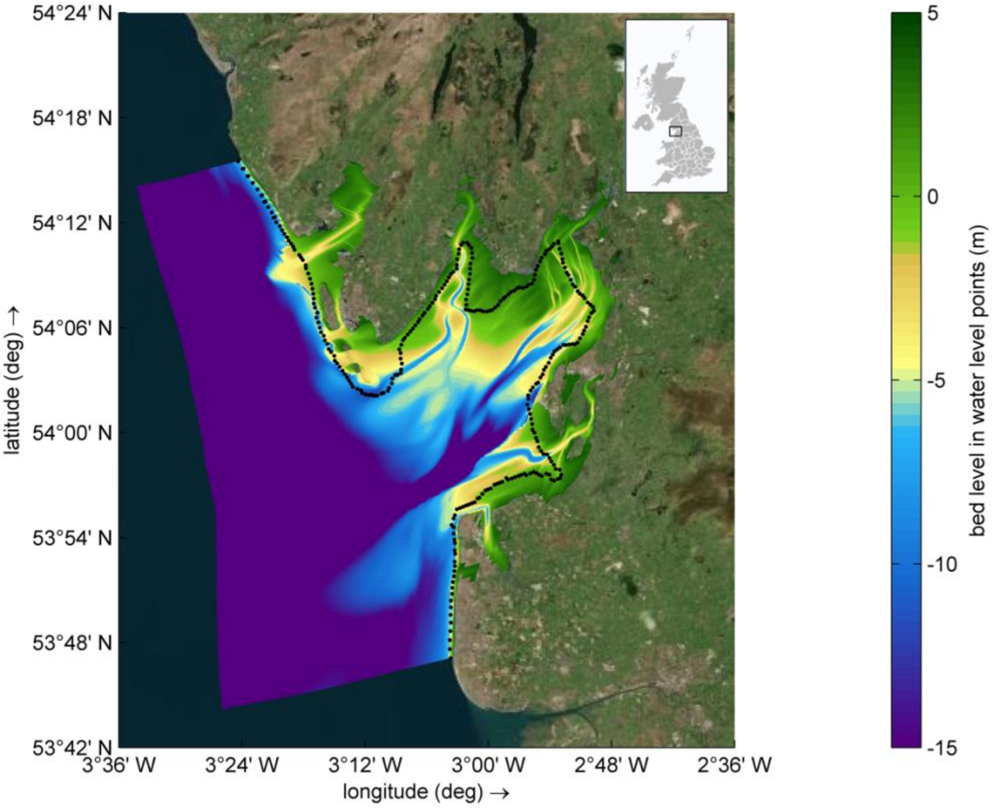

Fig. 1 Morecambe Bay model domain and bathymetry with observation points (circles)

Delft3D solves the 3-D Navier-Stokes equations for incompressible free-surface flow under the shallow water approximation for unsteady, incompressible, turbulent flow. The hydrodynamic and morphodynamic modules are fully coupled so that the flow field adjusts in real-time as the bed topography changes. The module Delft3D-WAVE can be then used to simulate wave generation, propagation, and nonlinear wave-wave interactions. Within this module, bottom dissipation, whitecapping, and depth induced breaking are fully accounted for in a dissipation term (Booij, Ris, & Holthuijsen, 1999).

Modeling results were recorded at 286 observation points along the Morecambe Bay shoreline, as presented in Fig 1. Artificial neural network (ANN) and Bayesian Network (BN) were trained to predict morphological changes and Depth Averaged Suspended Sediment Transport (SST).

ANN, sometime referred to as black-box (Akrami, El-Shafie, & Jaafar, 2013; Pavitra Kumar et al., 2021), mimics the human brain structure (El-Shafie, Noureldin, Taha, Hussain, & Mukhlisin, 2012; P. Kumar et al., 2020) to provide variables predictions through establishment of relationships between them and other pre-define inputs (Akrami et al., 2013). It has the capability of predicting non-linear variables and has found widespread application across physics and engineering (Arqub & Abo-Hammour, 2014). Fig 2. illustrates a basic ANN structures. ANN models receive inputs at the input layer which contains as many nodes as the number of inputs. Nodes in the input layer are connected to those of the hidden layer. As an example, the ANN in fig 2a consists of two hidden layers H_1 and H_2 containing 5 nodes each (N_1, N_2, N_3, N_4, and N_5). However, there can be any number of hidden layers with any number of nodes depending upon the level of complexity needed to deal with the inputs-outputs relationships. The hidden layer is followed by the output layer where the product of all the calculations within the network is provided (Fig 2a). The information received at the input layer is processed forward through the hidden layers to reach the output layer (El-Shafie & Noureldin, 2011). The structure of ANN shown in fig 2a is an example of Feed-Forward Neural Network (FFNN) where the information provided at the input layer flows forward from the input layer to the output layer. In contrast to feed-forward, fig 2b represents a Recurrent Neural Network (RNN) i.e., Elman Neural Network (ENN). In this case, a copy of the information flowing from input to output is diverted back in the hidden layers. ENN was designed for voice processing problems (Li et al., 2019) and is similar to the FFNN except for the addition of the context layer (Tampelini, Boscarioli, Peres, & Sampaio, 2011) which stores a copy of the information to be provided to the hidden layers in the subsequent calculation steps (Mahdaviani, Mazyar, Majidi, & Saraee, 2008). Each hidden layers have its own context layer with the number of nodes equal to the number of nodes in the corresponding hidden layer. The context layer acts as a memory to the ENN as it holds a copy of activations of previous time step (Sheela & Deepa, 2013).

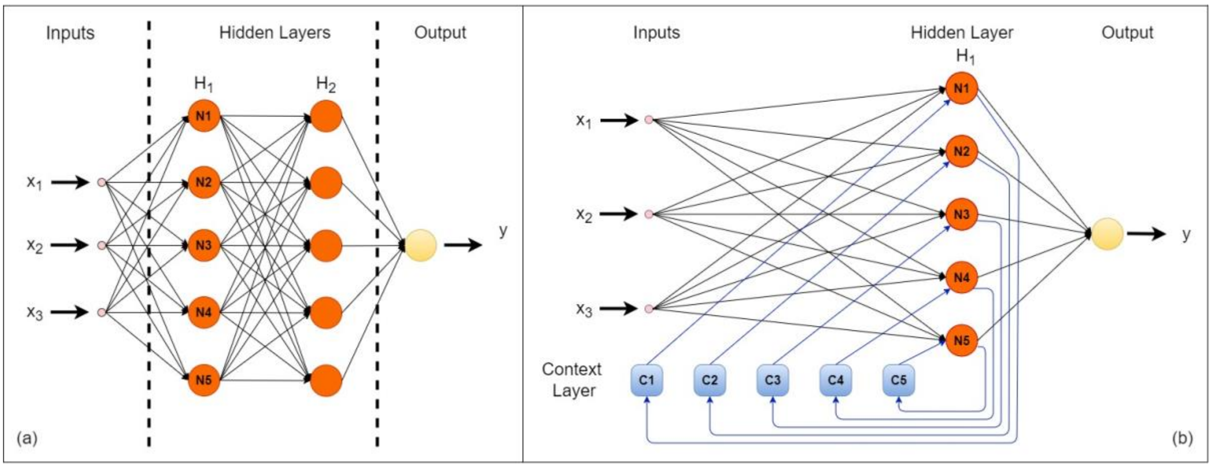

Fig. 2 Basic structure of ANN models (a) FFNN and (b) ENN

Bayesian Network is a statistical model which provides a framework for probabilistic prediction (Plant & Stockdon, 2012). BN evaluates the probability of a certain outcome based on prior probabilities developed by the network among the output and input variables. BN can use relationships and inductive reasoning to calculate the joint probability between the input variables (S. H. Chen & Pollino, 2012; Palmsten, Splinter, Plant, & Stockdon, 2014; Wilson, Adams, Hapke, Lentz, & Brenner, 2015). BN works on Bayes' theorem (Gutierrez, Plant, & Thieler, 2011) which provides a relation (eq. 1) to calculate the probability of occurrence of an event depending on the occurrence of other event(s) (Yates & Le Cozannet, 2012).

$$p(R_i|O_j) = \frac{p(O_j|R_i) \cdot p(R_i)}{p(O_j)} \tag{1}$$

$p(R_i|O_j)$ is the probability of the occurrence of event R_i, given a set of events O_j. Occurrence of an event can be joint occurrence of different events. For example, occurrence of the event "morphological change" is a joint occurrence of higher wave height and greater depth averaged velocity. The event scenarios i and j refers to the number of event R and observation O. $p(O_j|R_i)$ is said to be the likelihood of the set of observations (O) for the known event R, which represents the strength of the correlation between O and R. $p(R_i)$ is the prior probability of the event R. $p(O_i)$ is the likelihood of the observations.

2. Methods and Data

2.1 Simulation

Delft3D is used for simulating the hydrodynamics and morphdynamics of Morecambe Bay. The model grid has a varying resolution from around 120 x 200m onshore to around 1000 x 300m offshore. The bathymetry of Morecambe Bay (Fig 1) has been obtained from EDINA Marine Digimap download service (https://digimap.edina.ac.uk/roam/download/marine). DTM data from LiDAR surveys at 2 m resolution were then used for areas covering the shoreline and were downloaded from the UK Environment Agency's LiDAR data archive (https://environment.data.gov.uk/DefraDataDownload/?Mode=survey). The model boundary is forced with ten tidal harmonics (M2, S2, N2, K2, K1, O1, P1, Q1, S1, M4) interpolated across the two boundary extremes and derived from the global tidal model GOT-e 4.10c (Ray, 1999; Stammer et al., 2014). The model was calibrated using OpenDA and through comparison of the simulated water level values with values at the Heysham tidal station (https://ntslf.org/data/uk-network-real-time). The model was calibrated using OpenDA (Carnacina, Lima Rego, Verlaan, Zijl, & Van der Kaaij, 2015; Karri et al., 2013; Kurniawan, Ooi, Hummel, & Gerritsen, 2011; "OpenDA: Integrating models and observations,"). OpenDA interfaces with Delft3D and uses a derivative free algorithm (DUD or doesn't use derivative, Ralston and Jennrich, 1978), an algorithm for non-linear least squares minimization, to minimize a quadratic cost function based on differences between observed and model water levels through changing of roughness coefficient, water depth and boundary conditions. Successive iterations of the numerical simulation were repeated until the convergence criteria was reached. The accuracy was evaluated using the Brier Skill Score (Murphy and Epstein, 1989) defined as:

$$BSS = \frac{\alpha - \beta - \gamma + \varepsilon}{1 + \varepsilon} \tag{2}$$

where $\alpha = r_{XY}^2$, $\beta = \left(r_{XY} - \frac{\sigma_Y}{\sigma_X}\right)^2$, $\gamma = \left(\frac{\langle Y\rangle - \langle X\rangle}{\sigma_X}\right)^2$, $\varepsilon = \left(\frac{\langle X\rangle}{\sigma_X}\right)^2$ for which r is the correlation coefficient, σ is the standard deviation, ε is a normalization term, and X and Y are observed and modelled values. The model was calibrated from January 5th to February 20th, 2018 (Leonardi, 2022). The Brier Skill score in this case was 0.99. The model was subsequently run for 89 days, with a time step of 1 min from 1st of January to 30th March. The hydrodynamic model is fully coupled with a morphological model and the bathymetry is updated with a morphological scale factor of 10. The total morphological changes simulated with the factor of 10 for the whole simulation period (89 days in this case) is equivalent to morphological changes simulated for 10 times the original simulation period (i.e., 890 days). Non-Cohesive sediment type with specific density as 2650 kg/m^3 and dry bed density as 1600 kg/m^3 is used for simulating the sediment transportation. The initial sediment layer thickness at bed is set to 5m. Depth averaged (2DH) advection diffusion equation is solved for suspended sediment load calculation (Brakenhoff et al., 2020; Galappatti & Vreugdenhil, 1985). Van Rijn (1993) distinguished the bedload with suspended load based on a reference height (0.05m for this case), above which is considered as suspended load transport and below which is considered as bedload. The depth-averaged equilibrium concentration, solved using expressions provided by Van Rijn (2007), is used for calculation of sediment exchange between the bed and water column, which includes computation of velocity profile and vertical concentration profile. Near-bed reference concentration (C_a), computed by eq. 3, is required to compute the vertical sediment concentration profile.

$$C_a = 0.015\left(\frac{D_{50}}{a}\right)\frac{\left(\frac{\tau'_{b,cw} - \tau_{b,cr}}{\tau_{b,cr}}\right)^{1.5}}{D_*^{0.3}} \tag{3}$$

where: $\tau_{b,cr}$ is the critical bed shear stress, $\tau'_{b,cw}$ is grain related bed shear stress due to current and waves, D_{50} is median sediment diameter (120 µm, in this case), a is Van Rijn's reference height and D_* is non-dimensional grain size. The depth averaged suspended load transport is calculated by eq. 4.

$$\overrightarrow{q_s} = \vec{U} ch \tag{4}$$

where: $\overrightarrow{q_s}$ is depth averaged suspended sediment transport, $\vec{U}$ is depth averaged velocity, c is depth averaged sediment concentration and h is water depth.

Different boundary conditions were simulated by changing the significant wave height at the boundary (0.25m, 0.5m, 0.75m, 1m, 1.5m and 2m). Modelling results were recorded every ten minutes (simulated times) at 286 observation points plotted along the coastline at around 500m from each other (fig 1). The following variables were considered: Depth average velocity, Water depth, Significant Wave Height, Peak Wave Period, Wavelength, Cumulative Erosion/Sedimentation, and Depth Averaged Suspended Sediment Transport (SST). The time-series data of these variables from all 286 points and for all boundary forcing were then fed to ANN, ENN, and BN models in different format as required by these models for training.

2.2.1 Artificial Neural Network Modeling

The first set of ANN and ENN modeling was fed with modelling outputs time-series of Depth average velocity, Water depth, Significant Wave Height, Peak Wave Period, and Wavelength at the observation points as input to the models and target of the models were morphological changes and SST at the same observation points. For FFNN, data is divided into three datasets: training, testing, and validation dataset with corresponding percentage of 80, 10, and 10 percent (Gazzaz, Yusoff, Aris, Juahir, & Ramli, 2012), respectively. For ENN, data is divided into training and testing dataset with corresponding percentage of 80 and 20 percent (Y. Chen, Song, Liu, Yang, & Li, 2020; Liu, Yan, Tai, Xu, & Li, 2012). The training dataset is used for training the models i.e., updating the weights and biases of the network (de Gennaro et al., 2013; Najah, El-Shafie, Karim, & Jaafar, 2011). The validation dataset is used for preventing the overfitting of the model. Weights and biases are not updated in the validation process. Testing dataset is used for testing the final predictive strength of the model (P. Kumar et al., 2020). Training of ANN and ENN models requires a pre-defined configuration in terms of number of hidden layers and nodes because prediction accuracy of the model also depends on these factors. For instance, models having a smaller number of hidden layers and nodes fail to learn complete pattern of variations in the training dataset, thus lowering prediction accuracy. Similarly, models having greater number of hidden layers and nodes become more complex structure for the data with least variations leading to overfitting of the model, thus lowering prediction accuracy (Uzair & Jamil, 2020). Hence, an optimum number of hidden layers and its nodes are to be chosen for greater accuracy. In this study, training of FFNN and ENN models have been done on different combinations of hidden layers and nodes as presented in table 1. Optimum model, which provides better accuracy, is selected from these combinations based on the performance criteria. Training and analysis of FFNN and ENN models were done on MATLAB platform.

Table 1. Combination of hidden layers and nodes for FFNN and ENN

Model	**Hidden Layers**	**Number of nodes in Hidden layers**		
		H1	**H2**	**H3**
FFNN	2	10	10	-
	2	15	15	-
	2	20	20	-
	2	25	25	-
	3	10	10	10
	3	15	15	15
	3	20	20	20
	3	25	25	25
ENN	2	10	10	-
	2	15	15	-
	2	20	20	-
	2	25	25	-
	3	10	10	10
	3	15	15	15
	3	20	20	20
	3	25	25	25

2.2.2 Bayesian Modeling

The data received from Delft3D for Bayesian modeling is divided into two datasets: training and testing dataset with percentage division of 80 and 20 percent, respectively. Like the ANN modeling, Depth average velocity, Water depth, Significant Wave Height, Peak Wave Period, and Wavelength, are used as input to train the model for prediction of morphological changes, and SST. Each variable is represented by a node in BN (Gutierrez, Plant, Thieler, & Turecek, 2015; Zeigler et al., 2017). The joint correlation within the variables in BN ($P(E_i)$, $P(S_i)$) can be expressed as:

$$P(E_i) = \sum_{V,D,WH,WP,WL} P(E_i, V, D, WH, WP, WL) \quad (5)$$

$$P(S_i) = \sum_{V,D,WH,WP,WL} P(S_i, V, D, WH, WP, WL) \quad (6)$$

where E_i and S_i represents the probability of morphological change and SST, given the joint probability distribution with other variables (V: depth average velocity, D: water depth, WH: significant wave height, WP: peak wave period, WL: wavelength). The data for Bayesian modeling is divided into different bins for training. The number of bins selected for training determines the ability of the network to fit the data (Wang, Oldham, & Hipsey, 2016). For this study, input data was divided into 5 bins and target data was divided into two bin scenarios (Table 2). Training and analysis of these BN models were done using the Netica software package developed by Norsys Software Corporation.

Table 2. Classification of data into different number of bins

Mean Depth Average Velocity (m/s)	Mean Water depth (m)	Mean Wave Height (m)	Mean Wavelength (m)	Mean Wave Period (s)
<0.2	0 - 2	0 - 0.05	0 - 10	0 - 2

0.2 - 0.4	2 - 4	0.05 - 0.1	10 - 20	2 - 3
0.4 - 0.6	4 - 6	0.1 - 0.2	20 - 30	3 - 4
0.6 - 0.8	6 - 8	0.2 - 0.3	30 - 40	4 - 5
0.8 – 1.0	8 - 14	0.3 - 0.45	40 - 60	>5

Morphological change (m/year) (7 bins)	**SST ($m^3/s/m$) (7 bins)**	**Morphological change (m/year) (5 bins)**	**SST ($m^3/s/m$) (5 bins)**
<-2	0 – 0.0001	<-2	0 – 0.0001
-2 - -1	0.0001 – 0.0002	-2 - -1	0.0001 – 0.0002
-1 – 0	0.0002 – 0.0003	-1 – 1	0.0002 – 0.0004
0	0.0003 – 0.0004	1 – 2	0.0004 – 0.0006
0 - 1	0.0004 – 0.0005	>=2	>=0.0006
1 - 2	0.0005 – 0.0006	-	-
>=2	>=0.0006	-	-

2.3.1 Reduced Dependency Neural Networks modeling

Models developed in above sections are capable of predicting morphological changes and SST at the observation points along the coastline. But these models require input data such as Depth average velocity, Water depth, Significant Wave Height, Peak Wave Period, and Wavelength, at the same observation points for prediction and thus relies on localized data sources, which might not necessarily be easily available without an existing modelling run or data stations. Hence, this section proposes a model which was trained solely through boundary conditions of significant wave height, distance of the coastline from the boundary and angle of the coastline with respect to wave direction for prediction of morphological changes and SST at the observation points. The distance of each observation point from the boundary and the direction of the coastline in proximity of the observation point can be easily inferred from the geometry of the coastline though GIS. This set of reduced dependency models bypasses the need for numerical simulations and localized data sources. For this scenario, FFNN and ENN models were trained using the same data division percentage mentioned in the above sections and using the same sets of hidden layers and nodes as presented in table 1.

2.3.2 Reduced Dependency Bayesian modeling

Bayesian models were also developed using boundary conditions, distance and angle of the coastline as input variables. The joint correlation within the variables in BN is thus:

$$P(E_i) = \sum_{WH,Dt,A} P(E_i, WH, Dt, A) \quad (7)$$

$$P(S_i) = \sum_{WH,Dt,A} P(S_i, WH, Dt, A) \quad (8)$$

where E_i and S_i represents the probability of morphological changes rate and SST, given the joint probability distribution with other variables (WH: significant wave height, Dt: distance, A: angle of the coastline).

For training and analysis of these BN models, same data division process was followed as done in previous BN models. Number of bins for the target data was same as presented in table 2. However, the classification of inputs into number of bins were as presented in table 3.

Table 3. Classification of input data into different number of bins

Significant Wave Height (m)	**Distance (Km)**	**Angle (Degree)**
0.25	10 – 15	0 – 50
0.50	15 – 20	50 – 100
0.75	20 – 25	100 – 200
1.00	25 – 30	200 – 250
1.50	30 – 40	250 – 300
2.00	>=40	300 – 360

3. Performance Criteria

Prediction accuracy of ANN models is measured using regression, mean square error and Nash-Sutcliffe efficiency parameters (eq. 9, 10, and 11). The regression value is a statistical measure indicating how the data is fitting to its best fit line but does not reflect the deviation between predicted and target values. Hence, an additional parameters Mean Square Error (MSE) and Nash–Sutcliffe efficiency (NSE) were included to account the error in the predicted values. NSE measures the efficiency of the model on the scale of -∞ to 1, where 1 represents most efficient model. For BN models, the success percentage is used to measure the accuracy of the model, which indicates the number of correct bins predicted by the model over total number of attempts (eq. 12). The success percentage +/- 1 (eq. 11) bin indicates the total number of correct bin predictions plus the number of times the model has predicted bins immediately next to the correct ones.

Regression

$$r = \frac{n(\sum xy) - (\sum x)(\sum y)}{\sqrt{[n\sum x^2 - (\sum x)^2][n\sum y^2 - (\sum y)^2]}} \tag{9}$$

Mean Square Error

$$MSE = \frac{1}{n}\sum_{i=1}^{n}(x-y)^2 \tag{10}$$

Nash–Sutcliffe efficiency

$$NSE = 1 - \frac{\sum(y-x)^2}{\sum(x-\bar{x})^2} \tag{11}$$

Success Percentage

$$Sucess\ Percentage = \frac{Total\ number\ of\ currect\ bin\ prediction}{Total\ number\ of\ prediction\ attempts} * 100 \tag{12}$$

$$Sucess\ Percentage \pm 1\ bin = \frac{predictions\ (correct\ bins + next\ to\ correct\ bins)}{Total\ number\ of\ prediction\ attempts} * 100 \qquad (11)$$

4. Results

4.1 Simulation

Fig 3 provides an example of numerical modelling outputs at one of the 286 observation points (Fig 1). Modelling outputs were recorded every 10 minutes for the whole simulation period (89 days) and include: Depth average velocity, Water depth, Significant Wave Height, Peak Wave Period, Wavelength, Cumulative Erosion/Sedimentation, and SST. Cumulative Erosion/Sedimentation was converted to morphological change rate (m/y). The values of each time series were averaged and fed into the ANN and Bayesian models. The average values received from Delft3D was divided into three datasets (training, testing, and validation) for FFNN and two datasets (training and testing) for ENN. The division was such that all the datasets were statistically similar i.e., datasets have similar mean values. While dividing, it was ensured that the maximum and minimum values of the target data lie in the training dataset so that the models experience the extreme levels of the data pattern. FFNN and ENN models were trained with different number of hidden layers with different number of nodes in them. Separate models were trained for prediction of morphological change and SST. The results of the models trained for prediction of both morphological changes and SST are presented in table 4 and 5.

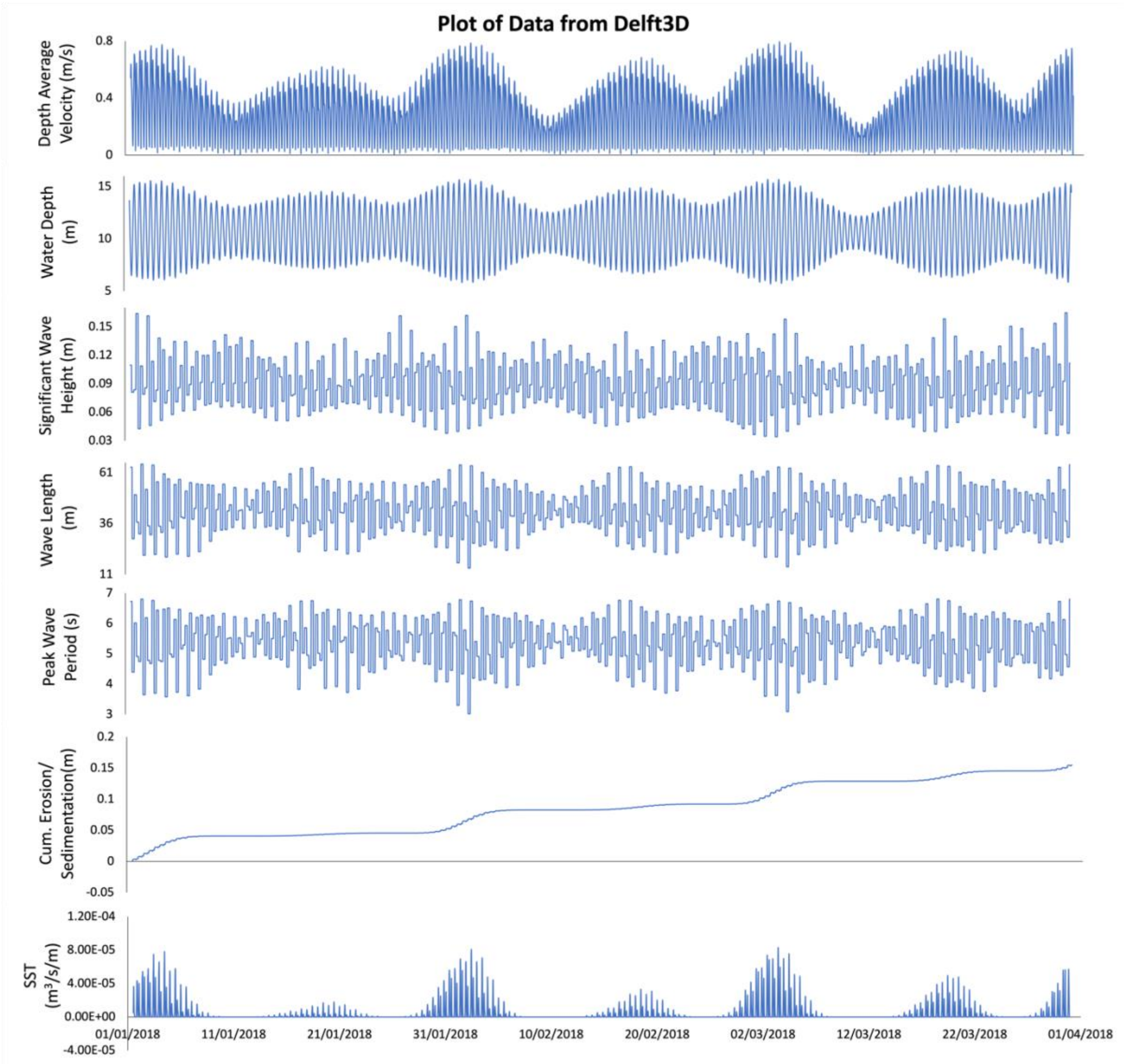

Fig. 3. Numerical modeling output

Table 4. Performance of FFNN and ENN models in predicting morphological changes

Model	Hidden Layers	Number of Nodes in Hidden Layer			Regression			Test MSE	NSE
		H1	H2	H3	Training	Validation	Testing		
FFNN	2	10	10	-	0.8931	0.8997	0.8856	0.1498	0.7969
	2	15	15	-	0.9394	0.9238	0.8985	0.1354	0.8723
	2	20	20	-	0.9356	0.9428	0.8889	0.1480	0.8679
	2	25	25	-	0.9201	0.9272	0.8992	0.1331	0.8442
	3	10	10	10	0.9196	0.8644	0.8836	0.1546	0.8261
	3	15	15	15	0.9324	0.9409	0.9074	0.1235	0.8667
	3	20	20	20	0.9295	0.9316	0.8914	0.1439	0.8578

	3	**25**	**25**	**25**	**0.9586**	**0.9385**	**0.9075**	**0.1254**	**0.9059**
ENN	2	10	10	-	0.9015	-	0.8320	0.2555	0.7871
	2	15	15	-	0.9485	-	0.8341	0.2561	0.8560
	2	20	20	-	0.9467	-	0.8415	0.2489	0.8551
	2	25	25	-	0.9656	-	0.8432	0.2472	0.8844
	3	10	10	10	0.9356	-	0.8505	0.2265	0.8441
	3	**15**	**15**	**15**	**0.9556**	**-**	**0.8643**	**0.2078**	**0.8790**
	3	20	20	20	0.9578	-	0.8454	0.2474	0.8722
	3	25	25	25	0.9639	-	0.8521	0.2432	0.8829

Models trained with different configuration have different level of accuracy (table 4). The training regression value varies from 0.8931 to 0.9586 for FFNN and 0.9015 to 0.9656 for ENN. However, the deciding parameter for model's strength is its testing results. The maximum testing regression obtained was 0.9075 with test mean square error as 0.1254 for FFNN and 0.8643 with test mean square error as 0.2078 for ENN. Hence, these two models were selected as optimum models providing better accuracy for prediction of morphological change. The optimum FFNN model has 3 hidden layers with 25 nodes each and optimum ENN model has the 3 hidden layers with 15 nodes each. The optimum models have acceptable NSE values of 0.9059 and 0.8790 for FFNN and ENN, respectively. ENN has its maximum training regression as 0.9656 but it has less testing regression and more testing mean square error in comparison to the selected optimum ENN model; hence, it was not considered fit to be chosen as optimum model. This is the case when model overfits. Overfitting of model is recognized when it performs well while training but cannot provide good results while testing (Ying, 2019). The regression plots containing training and testing regression plots of selected optimum FFNN, and ENN models are presented in fig 4.

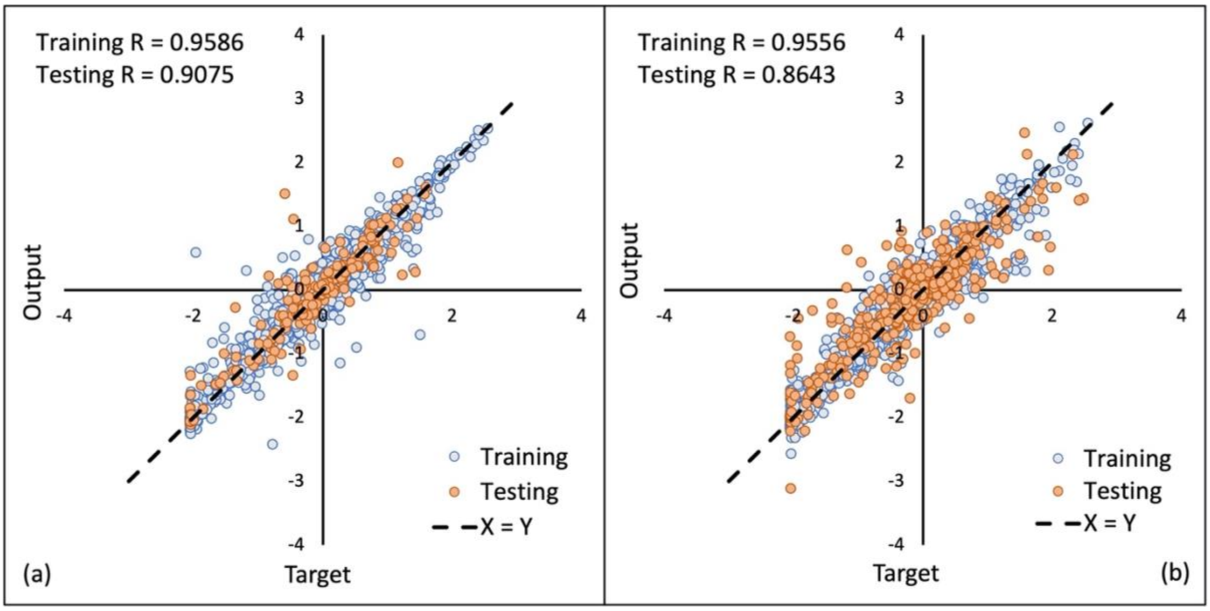

Fig. 4 Regression plot of (a) FFNN and (b) ENN optimum models for morphological change prediction

Table 5. Performance of FFNN and ENN models in predicting SST

Model	Hidden Layers	Number of Nodes in Hidden Layer			Regression			Test MSE	NSE
		H1	H2	H3	Training	Validation	Testing		
FFNN	2	10	10	-	0.9883	0.9910	0.9819	0.0030	0.9759
	2	15	15	-	0.9908	0.9922	0.9737	0.0045	0.9785
	2	20	20	-	0.9909	0.9917	0.9788	0.0037	0.9794
	2	**25**	**25**	**-**	**0.9928**	**0.9947**	**0.9852**	**0.0024**	**0.9846**
	3	10	10	10	0.9907	0.9929	0.9799	0.0033	0.9798
	3	15	15	15	0.9909	0.9941	0.9831	0.0029	0.9809
	3	20	20	20	0.9887	0.9908	0.9799	0.0033	0.9763
	3	25	25	25	0.9918	0.9937	0.9849	0.0026	0.9826
ENN	2	10	10	-	0.9913	-	0.9835	0.0031	0.9792
	2	15	15	-	0.9927	-	0.9824	0.0032	0.9813
	2	20	20	-	0.9961	-	0.9792	0.0037	0.9855
	2	**25**	**25**	**-**	**0.9939**	**-**	**0.9866**	**0.0024**	**0.9849**
	3	10	10	10	0.9932	-	0.9827	0.0031	0.9822
	3	15	15	15	0.9928	-	0.9850	0.0028	0.9824
	3	20	20	20	0.9949	-	0.9797	0.0036	0.9837
	3	25	25	25	0.9934	-	0.9860	0.0025	0.9839

SST values obtained from Delft3D were normalized within the range of -1 to 1 and all the training process and result analysis process were performed with the normalized data. The training and testing regression obtained for the model for predicting SST was about 0.99 and 0.98 (table 5), respectively, which represents a strong correlation between the input variables and SST. The optimum FFNN model, selected based on the testing results, has 2 hidden layers with 25 nodes each and provides training regression as 0.9928 and testing regression as 0.9852. It has the NSE value very close to 1 (0.9846) and testing mean square error as 0.0024. As mentioned earlier this mean square error is of the normalized data. The optimum ENN model, having 2 hidden layers with 25 nodes each, has similar training and testing accuracy with training regression as 0.9939 and testing regression as 0.9866 with testing mean square error as 0.0024 and NSE value of 0.9849. The maximum NSE value obtained by ENN models is 0.9855 but the corresponding testing MSE is greater than the selected optimum model, hence, it is not selected optimum model. The regression plots consisting of training and testing regression plots for optimum FFNN and ENN models for predicting SST are presented in fig 5.

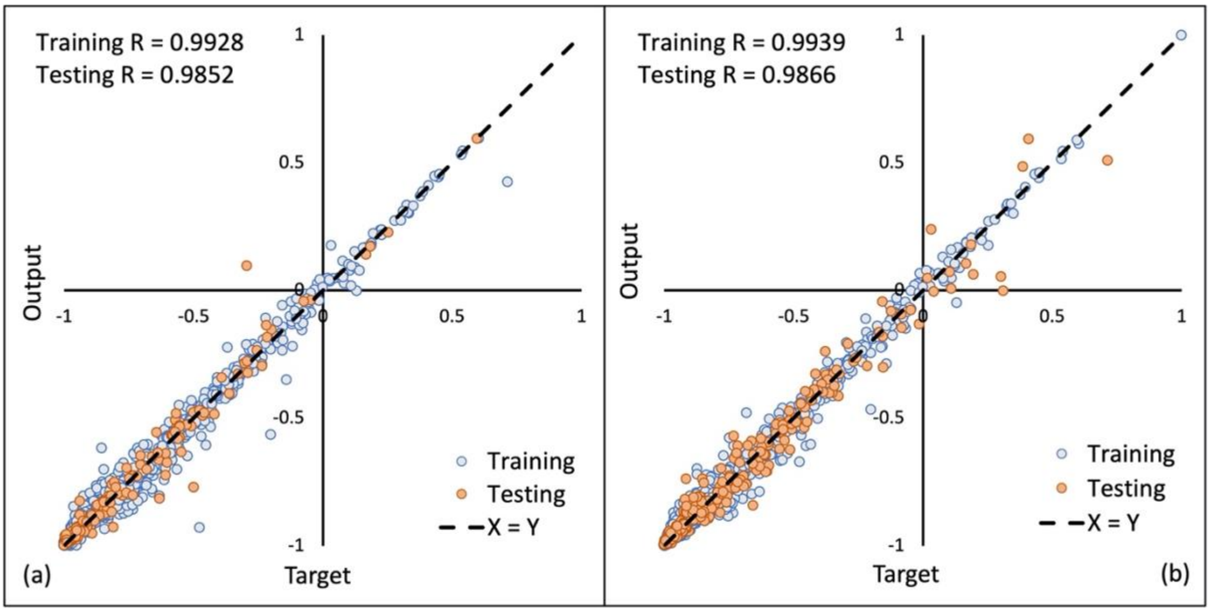

Fig. 5 Regression plots of (A) FFNN and (B) ENN optimum models for SST prediction

Fig 6 represents the Bayesian models developed for probabilistic prediction of morphological changes and SST with 7 bins (fig 6(a)) and 5 bins (fig 6(b)). As shown in fig 6, there are some connections within the input nodes. Mean depth-averaged velocity is depended on the mean depth at the observation points. Also, mean wave height, mean wavelength and mean wave height are inter-related. Hence, these nodes have connections within input nodes. Nodes contains the list of bins and corresponding prior probabilities (plotted next to it) (Plant et al., 2016), learned by the network from the training data. Like the ANN models, the data is divided into two sets: training and testing sets. Two BNs were trained by varying the number of bins in the target nodes from 5 to 7 while keeping the number of bins in the input nodes equal to 5. In Erosion/Accretion rate node with 7 bins, classification of bins is as: <-2 representing extreme erosion, -2 to -1 and -1 to 0 as moderate erosion, 0 as stable, 0 to 1 and 1 to 2 as moderate accretion and >=-2 as extreme accretion. The erosion rate/Accretion rate node with 5 bins has its classification as: <-2 represents the extreme erosion, -2 to -1 represents moderate erosion, -1 to 1 represents stable condition, 1 to 2 represents moderate accretion and >=2 represents extreme accretion. In similar fashion, bins of SST nodes are divided in 7 and 5 bins.

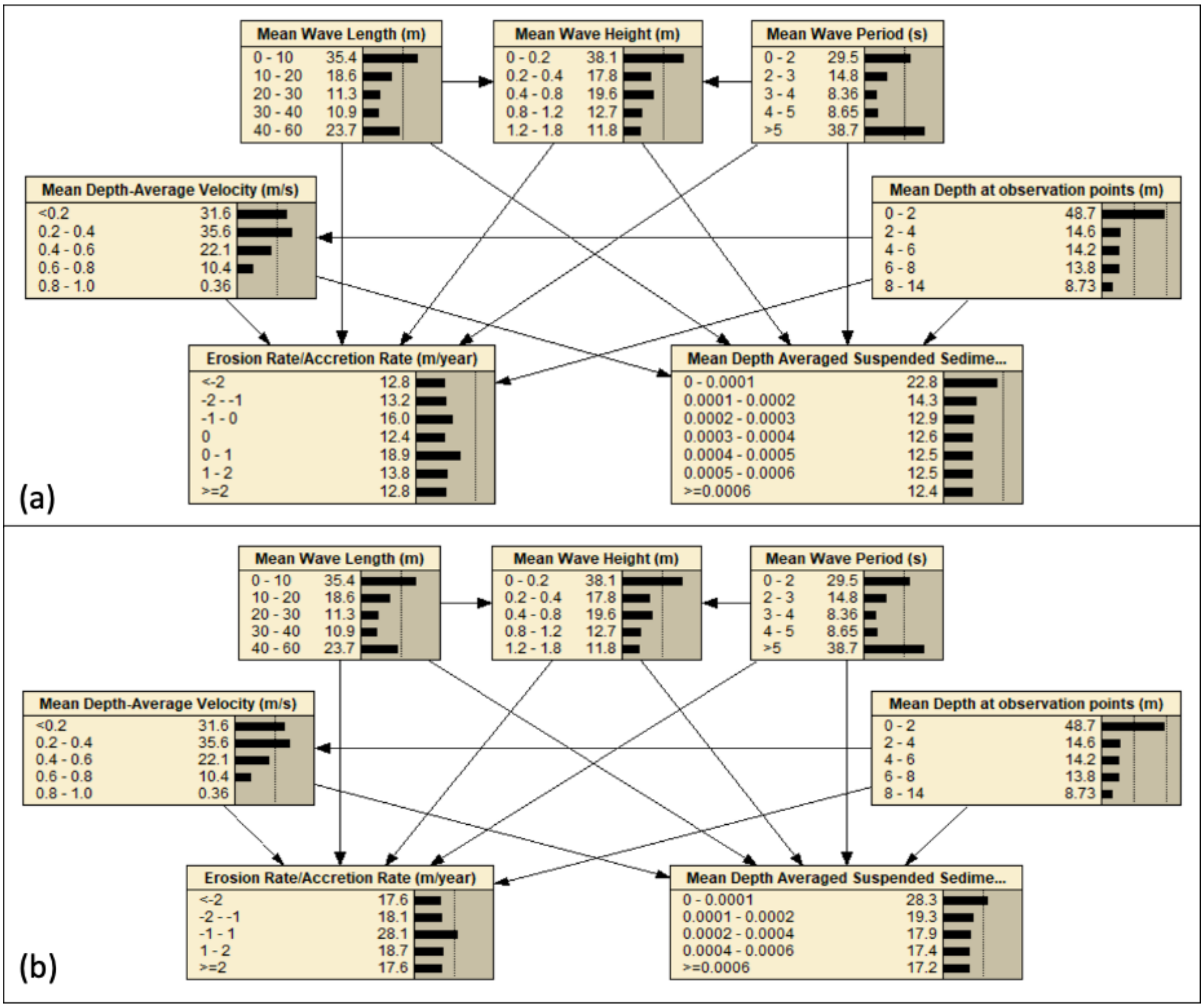

Fig. 6 Bayesian networks having (a) 7 bins and (b) 5 bins for prediction of morphological change and SST.

The results of BN trained and tested on the data from Delft3D are presented in table 6. The strength of the BN models is measured as the percentage success in predicting correct bins of morphological change and SST. There is significant increase in the percentage success when the bins are reduced by increasing the bin size. BN model has high percentage success rate in case of SST with 84.31% with 7 bins and 86.57% with 5 bins. Model was also performing good in its testing phase. BN model has high percentage success rate for morphological change prediction with 5 bins (81.97%) but has less percentage success rate when number of bins were increased to 7 bins (65.33%). Model performance improves when prediction of next to correct bin is counted as success prediction i.e., percentage success rate in +/- 1 bin is higher than the normal percentage success rate.

Table 6. Results of Bayesian models

Target	Number of Bins	Training		Testing	
		Percentage Success	Percentage Success +/- 1 bin	Percentage Success	Percentage Success +/- 1 bin
Morphological change	7	65.33	77.81	58.09	74.28
	5	81.97	95.84	76.88	94.51
SST	7	84.31	96.72	82.95	95.95
	5	86.57	97.96	84.97	97.40

4.3 Reduced Dependency Models

For the reduced dependency models, the training of FFNN and ENN was done using the same configurations as before but with limited input variables. These models were trained to predict morphological rates of change solely based on boundary condition values and basic geometrical features of the coastline. The optimum FFNN model for prediction of morphological change (table 7) has 2 hidden layers with 25 nodes each and provides the training regression of 0.8424 and testing regression of 0.7627 with testing mean square error of 0.3426 and NSE value as 0.6777. The optimum ENN model for prediction of morphological change (table 7) has 3 hidden layers with 15 nodes each and provides the training regression of 0.9022 and has the testing regression of 0.8358 with the testing mean square error of 0.2629 and NSE value as 0.7874. The regression plots of these two optimum models are presented in fig 7.

Table 7. Performance of FFNN and ENN models in predicting morphological change using boundary conditions

Model	Hidden Layers	Number of Nodes in Hidden Layer			Regression			Test MSE	NSE
		H1	H2	H3	Training	Validation	Testing		
FFNN	2	10	10	-	0.7775	0.7496	0.7438	0.3629	0.5932
	2	15	15	-	0.8944	0.8047	0.7283	0.4387	0.7488

	2	20	20	-	0.8663	0.7154	0.7219	0.4098	0.6981
	2	**25**	**25**	**-**	**0.8424**	**0.7337**	**0.7627**	**0.3426**	**0.6777**
	3	10	10	10	0.8525	0.7717	0.6801	0.4534	0.6834
	3	15	15	15	0.8478	0.7709	0.7722	0.3219	0.6937
	3	20	20	20	0.8920	0.7432	0.7129	0.4476	0.7339
	3	25	25	25	0.8483	0.6783	0.7196	0.4081	0.6666
ENN	2	10	10	-	0.8118	-	0.7942	0.3168	0.6517
	2	15	15	-	0.8350	-	0.7923	0.3186	0.6814
	2	20	20	-	0.8761	-	0.8164	0.2868	0.7444
	2	25	25	-	0.8851	-	0.8047	0.3199	0.7491
	3	10	10	10	0.8465	-	0.8217	0.2782	0.7066
	3	**15**	**15**	**15**	**0.9022**	**-**	**0.8358**	**0.2629**	**0.7874**
	3	20	20	20	0.9275	-	0.7835	0.3728	0.7965
	3	25	25	25	0.9172	-	0.8260	0.2847	0.8036

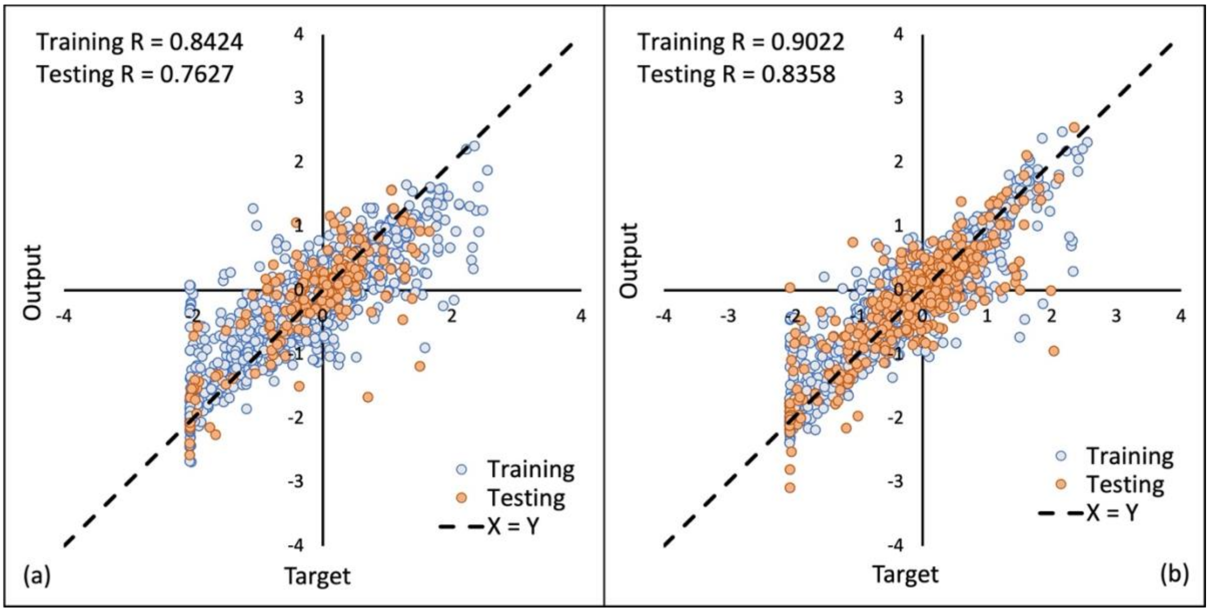

Fig. 7 Regression plots for (a) FFNN and (b) ENN models for prediction of morphological changes using boundary conditions

Models for prediction of SST based on the boundary condition values and basic geometrical features of the coastline were trained on the same configuration and same normalized data as in previous paragraphs. The optimum FFNN model for prediction of SST (table 8) has 2 hidden layers with 15 nodes each and provides the training regression of 0.9704 and testing regression of 0.9538 with the testing mean square error of 0.0085 and NSE value as 0.9347. The optimum ENN model for prediction of SST (table 8) has 3 hidden layers with 25 nodes each and provides the training regression of 0.9367 and testing regression of 0.8801 with testing mean square error of 0.0205 and NSE value as 0.8562. Fig 8 represents the regression plot of these two optimum models.

Table 8. Performance of FFNN and ENN models in predicting SST using boundary conditions

Model	**Hidden Layers**	**Number of Nodes in Hidden Layer**			**Regression**			**Test MSE**	**NSE**
		H1	**H2**	**H3**	**Training**	**Validation**	**Testing**		
FFNN	2	10	10	-	0.9230	0.9173	0.9224	0.0138	0.8506
	2	**15**	**15**	**-**	**0.9704**	**0.9535**	**0.9538**	**0.0085**	**0.9347**
	2	20	20	-	0.9504	0.9281	0.9479	0.0097	0.8973
	2	25	25	-	0.8791	0.8735	0.8581	0.0313	0.7498
	3	10	10	10	0.9545	0.9168	0.9293	0.0130	0.8981
	3	15	15	15	0.9510	0.9405	0.9355	0.0116	0.8973
	3	20	20	20	0.9365	0.9277	0.9187	0.0153	0.8689
	3	25	25	25	0.8954	0.8954	0.8798	0.0240	0.7892
ENN	2	10	10	-	0.8811	-	0.8493	0.0254	0.7646
	2	15	15	-	0.8847	-	0.7935	0.0344	0.7480
	2	20	20	-	0.9249	-	0.8002	0.0333	0.8103
	2	25	25	-	0.8855	-	0.8003	0.0329	0.7541
	3	10	10	10	0.9345	-	0.8670	0.0224	0.8488
	3	15	15	15	0.9378	-	0.8392	0.0286	0.8401
	3	20	20	20	0.9346	-	0.8818	0.0205	0.8531
	3	**25**	**25**	**25**	**0.9367**	**-**	**0.8801**	**0.0205**	**0.8562**

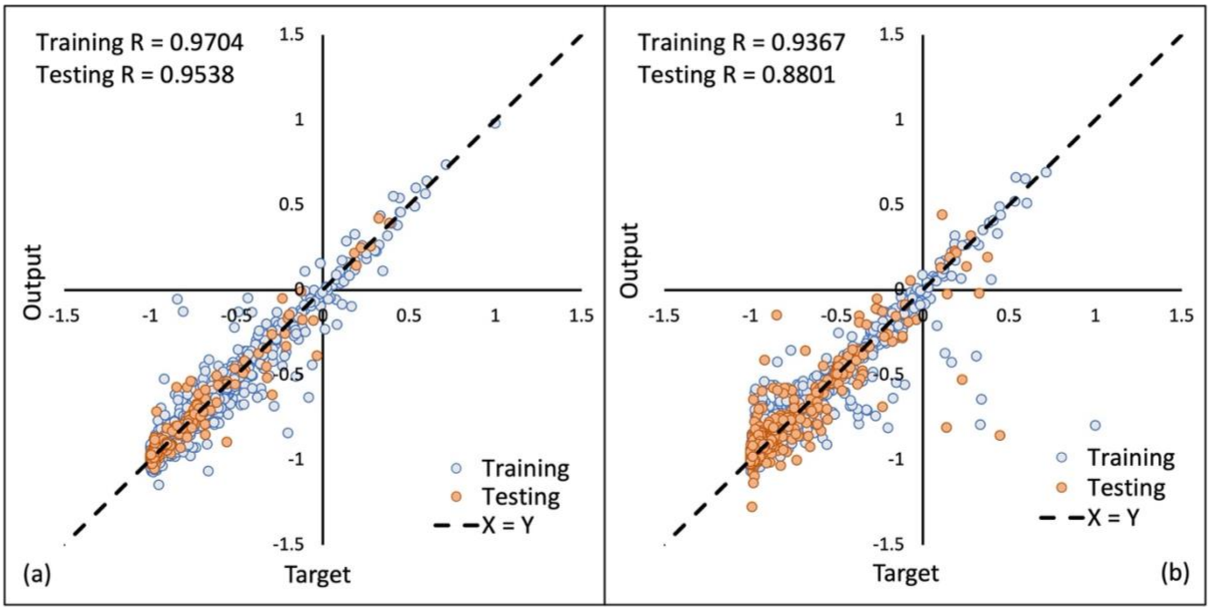

Fig. 8 Regression plots for (a) FFNN and (b) ENN models for prediction of SST using boundary conditions

Fig 9 represents the BN models trained for prediction of morphological changes and SST using 7 bins and 5 bin, respectively. Process of classification of bins for the target nodes were same as that followed in earlier BN models. The bins of input nodes (wave height, distance, and angle) were classified based on the limits of the data available for training. The probabilities of bins displayed in fig 9 is the prior probabilities learned by the network based on the training data.

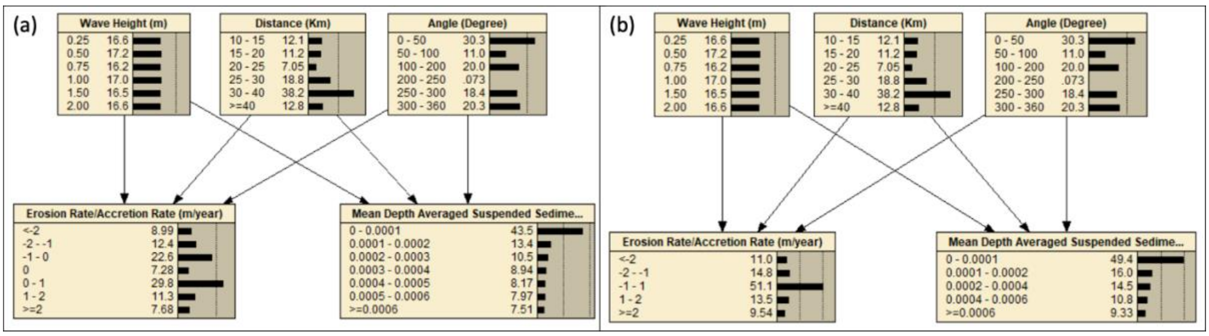

Fig. 9 Bayesian networks having (A) 7 bins and (B) 5 bins for prediction of morphological change and SST

Table 9 presents the result of the BN models trained using boundary data. The maximum percentage success rate obtained was 77.88% for morphological change prediction with testing percentage success rate of 78.61% with 5 bins. Percentage success rate increased to 95.40% for training and to 96.82% for testing when +/- 1 bin is included. However, for SST percentage success rate increased slightly for 5 bins (74.60%) when compared to 7 bins (73.58%).

Table 9. Results of Bayesian models trained using boundary conditions

Target	Number of Bins	Training		Testing	
		Percentage Success	**Percentage Success +/- 1 bin**	**Percentage Success**	**Percentage Success +/- 1 bin**
Morphological change	7	59.27	72.63	51.73	64.74
	5	77.88	95.40	78.61	96.82
SST	7	73.58	88.10	71.97	88.44
	5	74.60	89.27	73.12	89.31

5. Discussion

This article is proposing FFNN, ENN and BN models for prediction of morphological change and SST at the coastline based on only the boundary condition values and basic geometrical features of the coastline. Comparison of the accuracy of all the models is presented in table 10.

Table 10. Comparison of all models

Target	Model	Training		Testing		MSE
		Regression/ Percentage Success	**Percentage Success +/- 1 bin**	**Regression/ Percentage Success**	**Percentage Success +/- 1 bin**	
Models on Localised data source						
Morpho-logical change	FFNN	0.9586	-	0.9075	-	0.1254
	ENN	0.9556	-	0.8643	-	0.2078
	BN (7 bin)	65.33	77.81	58.09	74.28	-
	BN (5 bin)	81.97	95.84	76.88	94.51	-
SST	FFNN	0.9928	-	0.9852	-	0.0024
	ENN	0.9939	-	0.9866	-	0.0024
	BN (7 bin)	84.31	96.72	82.95	95.95	-

	BN (5 bin)	86.57	97.96	84.97	97.40	-
Models on Boundary Conditions						
Morpho-logical change	FFNN	0.8944	-	0.7283	-	0.4387
	ENN	0.9172	-	0.8260	-	0.2847
	BN (7 bin)	59.27	72.63	51.73	64.74	-
	BN (5 bin)	77.88	95.40	78.61	96.82	-
SST	FFNN	0.9704	-	0.9538	-	0.0085
	ENN	0.9367	-	0.8801	-	0.0205
	BN (7 bin)	73.58	88.10	71.97	88.44	-
	BN (5 bin)	74.60	89.27	73.12	89.31	-

Optimum FFNN and ENN models seems to have similar regression values. Hence, any model can be used for prediction of morphological change and SST. However, it is recommended to use both FFNN and ENN models and average the outputs, which will create an ensemble effect, and thus, will help in reducing the final output error (Yang & Browne, 2004). BN models with 7 bins in target nodes have lower percentage success rates than that with 5 bins. Creating a greater number of bins reduces the size of each bin. Classifying bins with reduced size (lower range) is a tough task for models, thus, reducing the percentage success rate. However, creating too few bins reduces the usability of the model. For instance, a model having only two bins (erosion vs accretion) will have greater percentage success rate but will provide less information in comparison to models having a number of bins sufficient to identify conditions of moderate, severe or stable morphological changes. Thus, a model with 5 bins is considered adequate as it can provide prediction of sever erosion rate (<-2 m/year), moderate erosion rate (-2 to -1 m/year), stable (-1 to 1 m/year), moderate accretion (1 to 2 m/year) and sever accretion (>2 m/year). BN models with 5 bins trained on the localized data at observation points have percentage success rate greater than 80% in training and greater than 75% in testing. When measured with +/- 1 bins the percentage success is greater than 94%. BN models trained on boundary data have percentage success rate greater than 73%, which is acceptable being this, to our knowledge, the first attempt in literature of developing predictive data-driven modelling using solely boundary data and coastline features. FFNN, ENN and BN models, trained in this study, have comparable or higher accuracy with respect to BN models previously developed for prediction of shoreline change. Plant et al. (2016) proposed BN model for prediction of shoreline change in the Gulf of Mexico. The prediction skill of BN obtained for prediction of shoreline change was 0.6. Yates and Le Cozannet (2012) proposed BN model for evaluating the European coastline evolution which was accurately reproducing more than 65% of shoreline evolution trend. The BN models proposed in this study has the percentage success rate more than 73% in predicting morphological changes and SST at Morecambe Bay.

The prediction models proposed in this study have the advantage, over other morphological change and SST predicting models, of eliminating the dependency on localized data. Once trained, these models can predict morphological evolution based on boundary conditions of significant wave height, distance of the coastline from the boundary and angle of the coastline with respect to wave direction. The limitation of these models is that they are site-specific (Cabaneros, Calautit, & Hughes, 2017), i.e., these models provide accurate predictions only for the location where models have been trained on. For this study, the data used for FFNN, ENN and BN training was simulated for Morecambe Bay, hence, these models will provide accurate predictions for Morecambe Bay only. For predictions at other coasts these models need to be re-configured and re-trained on the data patterns of that coasts. ANN and BN models have an advantage in terms of computational time with respect to a full hydro-morphodynamical models. The latter can require several hours of computational time. ANN and BN models, once trained, can predict the morphological changes close to simulated values within the order of a few minutes, saving time and computational resources.

6. Conclusion

This article proposes two set of FFNN, ENN and BN models: one set trained on localized modelling outputs or localized data sources and one having reduced dependency from modelling outputs and, once trained, solely relying on boundary conditions and coastline geometry. The morphological change and SST data for training the models are obtained from simulation for Morecambe Bay on Delft3D software package. These data are simulated for 89 days and are recorded at an interval of 10 min along with other input data. Simulated input variables are Depth average velocity, Water depth, Significant Wave Height, Peak Wave Period, and Wavelength. These input and target data are transformed into the required format for training FFNN, ENN and BN models. FFNN and ENN models trained on localized data at observation points provide training regression greater than 0.95 and testing regression greater than 0.86. BN models, when trained with 5 bins, provide higher percentage success rate which is greater than 80% for training and greater than 76% for testing. FFNN and ENN models trained on boundary conditions, provide regression values greater than 0.84 for training and greater than 0.76 for testing. BN model with 5 bins trained on boundary conditions provide percentage success rate greater than 74% for training and greater than 73% for testing. These models provide sufficient accuracy for prediction of morphological change and SST. FFNN and ENN models, for this study, are providing similar regression values. Hence, it is recommended to use both the models for prediction and average the outputs, which will provide more accurate morphological change and SST values. For future studies, it is recommended to further improve the accuracy of the models trained on boundary conditions by adding more relevant input variables upon which the morphological change and SST depends.

Acknowledgments

We acknowledge the following funding source for this study: Engineering with Nature: combining Artificial intelligence, Remote sensing and computer Models for the optimum design of coastal protection schemes EP/V056042/1. **Data Access Statement**: Bathymetry data have been retrieved from EDINA Marine Digimap (https://digimap.edina.ac.uk/roam/download/marine) and UK Environment Agency's LiDAR data archive (https://environment.data.gov.uk/DefraDataDownload/?Mode=survey) which are gratefully acknowledged. The Data drive models have been developed using the following which are also acknowledged: MATLAB libraries from the Deep Learning toolbox (e.g. *feedforwardnet()*, *elmannet()* and *train()*) and Netica software (free-version) developed by Norsys software corp.

Reference:

Akrami, S. A., El-Shafie, A., & Jaafar, O. (2013). Improving Rainfall Forecasting Efficiency Using Modified Adaptive Neuro-Fuzzy Inference System (MANFIS). *Water Resour Manage*. doi:10.1007/s11269-013-0361-9

Arqub, O. A., & Abo-Hammour, Z. (2014). Numerical solution of systems of second-order boundary value problems using continuous genetic algorithm. *Information Sciences*. doi:10.1016/j.ins.2014.03.128

Booij, N., Ris, R. C., & Holthuijsen, L. H. (1999). A third-generation wave model for coastal regions: 1. Model description and validation. *Journal of Geophysical Research: Oceans, 104*(C4), 7649-7666. doi:https://doi.org/10.1029/98JC02622

Brakenhoff, L., Schrijvershof, R., van der Werf, J., Grasmeijer, B., Ruessink, G., & van der Vegt, M. (2020). From Ripples to Large-Scale Sand Transport: The Effects of Bedform-Related Roughness on Hydrodynamics and Sediment Transport Patterns in Delft3D. *Journal of Marine Science and Engineering, 8*(11), 892. Retrieved from https://www.mdpi.com/2077-1312/8/11/892

Buchholz, K. (2020). Rising Sea Levels Will Threaten 200 Million People by 2100. Retrieved from https://www.statista.com/chart/19884/number-of-people-affected-by-rising-sea-levels-per-country/

Cabaneros, S. M. S., Calautit, J. K. S., & Hughes, B. R. (2017). Hybrid Artificial Neural Network Models for Effective Prediction and Mitigation of Urban Roadside NO2 Pollution. *Energy Procedia, 142*, 3524-3530. doi:https://doi.org/10.1016/j.egypro.2017.12.240

Carnacina, I., Lima Rego, J., Verlaan, M., Zijl, F., & Van der Kaaij, T. (2015). *The 2013 Xaver storm surge and the resilient response of the North Sea defense system*. Paper presented at the 36th IAHR World Congress, Madrid, Spain.

Chen, C., Qi, J., Liu, H., Beardsley, R. C., Lin, H., & Cowles, G. (2022). A Wet/Dry Point Treatment Method of FVCOM, Part I: Stability Experiments. *Journal of Marine*

Science and Engineering, 10(7), 896. Retrieved from https://www.mdpi.com/2077-1312/10/7/896

Chen, S. H., & Pollino, C. A. (2012). Good practice in Bayesian network modelling. *Environmental Modelling & Software, 37*, 134-145. doi:https://doi.org/10.1016/j.envsoft.2012.03.012

Chen, Y., Song, L., Liu, Y., Yang, L., & Li, D. (2020). A Review of the Artificial Neural Network Models for Water Quality Prediction. *Applied Sciences, 10*(17), 5776. Retrieved from https://www.mdpi.com/2076-3417/10/17/5776

Ciavola, P., Ferreira, O., Haerens, P., Van Koningsveld, M., Armaroli, C., & Lequeux, Q. (2011). Storm impacts along European coastlines. Part 1: The joint effort of the MICORE and ConHaz Projects. *Environmental Science & Policy, 14*(7), 912-923. doi:https://doi.org/10.1016/j.envsci.2011.05.011

Dawson, R. J., Thompson, D., Johns, D., Gosling, S., Chapman, L., Darch, G., . . . Wood, R. (2016). *UK Climate Change Risk Assessment Evidence Report: Chapter 4, Infrastructure*. Retrieved from https://www.theccc.org.uk/wp-content/uploads/2016/07/UK-CCRA-2017-Chapter-4-Infrastructure.pdf

de Gennaro, G., Trizio, L., Di Gilio, A., Pey, J., Perez, N., Cusack, M., . . . Querol, X. (2013). Neural network model for the prediction of PM10 daily concentrations in two sites in the Western Mediterranean. *Sci Total Environ, 463-464*, 875-883. doi:10.1016/j.scitotenv.2013.06.093

Deutz, A., Kellett, J., & Zoltani, J. (2018). Innovative Finance for Resilient Coasts and Communities. *United Nations Development Programme and The Nature Conservancy*. Retrieved from www.nature.org/content/dam/tnc/nature/en/documents/Innovative_Finance_Resilient_Coasts_and_Communities.pdf

El-Shafie, A., & Noureldin, A. (2011). Generalized versus non-generalized neural network model for multi-lead inflow forecasting at Aswan High Dam. *Hydrol. Earth Syst. Sci., 15*(3), 841-858. doi:10.5194/hess-15-841-2011

El-Shafie, A., Noureldin, A., Taha, M., Hussain, A., & Mukhlisin, M. (2012). Dynamic versus static neural network model for rainfall forecasting at Klang River Basin, Malaysia. *Hydrol. Earth Syst. Sci.*, 1151-1169. doi:10.5194/hess-16-1151-2012

Galappatti, G., & Vreugdenhil, C. (1985). A depth-integrated model for suspended sediment transport. *Journal of Hydraulic Research, 23*(4), 359-377.

Gazzaz, N. M., Yusoff, M. K., Aris, A. Z., Juahir, H., & Ramli, M. F. (2012). Artificial neural network modeling of the water quality index for Kinta River (Malaysia) using water quality variables as predictors. *Marine Pollution Bulletin, 64*(11), 2409-2420. doi:https://doi.org/10.1016/j.marpolbul.2012.08.005

Gutierrez, B. T., Plant, N. G., & Thieler, E. R. (2011). A Bayesian network to predict coastal vulnerability to sea level rise. *Journal of Geophysical Research: Earth Surface, 116*(F2). doi:https://doi.org/10.1029/2010JF001891

Gutierrez, B. T., Plant, N. G., Thieler, E. R., & Turecek, A. (2015). Using a Bayesian network to predict barrier island geomorphologic characteristics. *Journal of Geophysical Research: Earth Surface, 120*(12), 2452-2475. doi:https://doi.org/10.1002/2015JF003671

Huang-Lachmann, J.-T., & Lovett, J. C. (2016). How cities prepare for climate change: Comparing Hamburg and Rotterdam. *Cities, 54*, 36-44. doi:https://doi.org/10.1016/j.cities.2015.11.001

Karri, R. R., Badwe, A., Wang, X., El Serafy, G., Sumihar, J., Babovic, V., & Gerritsen, H. (2013). Application of data assimilation for improving forecast of water levels and residual currents in Singapore regional waters. *Ocean Dynamics, 63*(1), 43-61. doi:10.1007/s10236-012-0584-y

King, E. V., Conley, D. C., Masselink, G., Leonardi, N., McCarroll, R. J., Scott, T., & Valiente, N. G. (2021). Wave, tide and topographical controls on headland sand bypassing. *Journal of Geophysical Research: Oceans*, *126*(8), e2020JC017053.

Kumar, P., Lai, S. H., Mohd, N. S., Kamal, M. R., Afan, H. A., Ahmed, A. N., . . . El-Shafie, A. (2020). Optimised neural network model for river-nitrogen prediction utilizing a new training approach. *PLoS One, 15*(9), e0239509. doi:10.1371/journal.pone.0239509

Kumar, P., Lai, S. H., Mohd, N. S., Kamal, M. R., Ahmed, A. N., Sherif, M., . . . El-shafie, A. (2021). Enhancement of nitrogen prediction accuracy through a new hybrid model using ant colony optimization and an Elman neural network. *Engineering Applications of Computational Fluid Mechanics, 15*(1), 1843-1867. doi:10.1080/19942060.2021.1990134

Kurniawan, A., Ooi, S. K., Hummel, S., & Gerritsen, H. (2011). Sensitivity analysis of the tidal representation in Singapore Regional Waters in a data assimilation environment. *Ocean Dynamics, 61*(8), 1121-1136. doi:10.1007/s10236-011-0415-6

Leonardi, 2022, Modelling of Intertidal Sediment Transport in a Macrotidal Embayment Proceedings of the 39th IAHR World Congress, 19–24 June 2022, Granada, Spain, doi://10.3850/IAHR-39WC2521716X20221050

Li, C., Zhu, L., He, Z., Gao, H., Yang, Y., Yao, D., & Qu, X. (2019). Runoff Prediction Method Based on Adaptive Elman Neural Network. *Water (MDPI), 11*, 1113. doi:10.3390/w11061113

Liu, S., Yan, M., Tai, H., Xu, L., & Li, D. (2012, 2012//). *Prediction of Dissolved Oxygen Content in Aquaculture of Hyriopsis Cumingii Using Elman Neural Network.* Paper presented at the Computer and Computing Technologies in Agriculture V, Berlin, Heidelberg.

Lyddon, C. E., Brown, J. M., Leonardi, N., Saulter, A., & Plater, A. J. (2019). Quantification of the uncertainty in coastal storm hazard predictions due to wave-current interaction and wind forcing. *Geophysical Research Letters*, *46*(24), 14576-14585.

López, I., Aragonés, L., Villacampa, Y., & Compañ, P. (2018). Artificial neural network modeling of cross-shore profile on sand beaches: The coast of the province of Valencia (Spain). *Marine Georesources & Geotechnology, 36*(6), 698-708. doi:10.1080/1064119X.2017.1385666

Mahdaviani, K., Mazyar, H., Majidi, S., & Saraee, M. H. (2008). *A Method to Resolve the Overfitting Problem in Recurrent Neural Networks for Prediction of Complex Systems' Behavior*. Paper presented at the International Joint Conference on Neural Networks (IJCNN 2008).

Mason, D. C., Scott, T. R., & Dance, S. L. (2010). Remote sensing of intertidal morphological change in Morecambe Bay, U.K., between 1991 and 2007. *Estuarine, Coastal and Shelf Science, 87*(3), 487-496. doi:https://doi.org/10.1016/j.ecss.2010.01.015

Muñoz, D. F., Yin, D., Bakhtyar, R., Moftakhari, H., Xue, Z., Mandli, K., & Ferreira, C. (2022). Inter-Model Comparison of Delft3D-FM and 2D HEC-RAS for Total Water Level Prediction in Coastal to Inland Transition Zones. *JAWRA Journal of the American Water Resources Association, 58*(1), 34-49. doi:https://doi.org/10.1111/1752-1688.12952

Najah, A., El-Shafie, A., Karim, O. A., & Jaafar, O. (2011). Integrated versus isolated scenario for prediction dissolved oxygen at progression of water quality monitoring stations. *Hydrol. Earth Syst. Sci., 15*, 2693-2708. doi:10.5194/hess-15-2693-2011

Nunez, C., & Staff, N. G. (2022). Sea level rise, explained. Retrieved from https://www.nationalgeographic.com/environment/article/sea-level-rise-1

OpenDA: Integrating models and observations. Retrieved from http://www.openda.org

Palmsten, M. L., Splinter, K. D., Plant, N. G., & Stockdon, H. F. (2014). Probabilistic estimation of dune retreat on the Gold Coast, Australia. *Shore Beach, 82*(4), 35-43. Retrieved from https://www.scopus.com/inward/record.uri?eid=2-s2.0-84930684591&partnerID=40&md5=bcb1d14a4da8412acad18b843410730f

Plant, N. G., Robert Thieler, E., & Passeri, D. L. (2016). Coupling centennial-scale shoreline change to sea-level rise and coastal morphology in the Gulf of Mexico using a Bayesian network. *Earth's Future, 4*(5), 143-158. doi:https://doi.org/10.1002/2015EF000331

Plant, N. G., & Stockdon, H. F. (2012). Probabilistic prediction of barrier-island response to hurricanes. *Journal of Geophysical Research: Earth Surface, 117*(F3). doi:https://doi.org/10.1029/2011JF002326

Ray, R. D. (1999). A Global Ocean Tide Model From TOPEX/POSEIDON Altimetry: GOT99.2. *NASA Tech. Memo.*, 58.

Rodriguez-Delgado, C., Bergillos, R. J., & Iglesias, G. (2019). An artificial neural network model of coastal erosion mitigation through wave farms. *Environmental Modelling & Software, 119*, 390-399. doi:https://doi.org/10.1016/j.envsoft.2019.07.010

Shchepetkin, A. F., & McWilliams, J. C. (2005). The regional oceanic modeling system (ROMS): a split-explicit, free-surface, topography-following-coordinate oceanic model. *Ocean Modelling, 9*(4), 347-404. doi:https://doi.org/10.1016/j.ocemod.2004.08.002

Sheela, K. G., & Deepa, S. N. (2013). Review on Methods to Fix Number of Hidden Neurons in Neural Networks. *Hindawi Publishing Corporation, Mathematical Problems in Engineering, 2013*. doi:10.1155/2013/425740

Stammer, D., Ray, R. D., Andersen, O. B., Arbic, B. K., Bosch, W., Carrère, L., . . . Yi, Y. (2014). Accuracy assessment of global barotropic ocean tide models. *Reviews of Geophysics, 52*(3), 243-282. doi:https://doi.org/10.1002/2014RG000450

Sumangala, D., & Warrior, H. (2022). Coastal modelling incorporating artificial neural networks for improved velocity prediction. *ISH Journal of Hydraulic Engineering, 28*(sup1), 261-271. doi:10.1080/09715010.2020.1771220

Tampelini, L. G., Boscarioli, C., Peres, S. M., & Sampaio, S. C. s. (2011). An application of Elman networks in treatment and prediction of hydrologic time series. *Journal of the Brazilian Neural Network Society, 9*(3), 148-156. doi:10.21528/LNLM-vol9-no3-art1

UNCC. (2020). *Policy brief: Technologies for Averting, Minimizing and Addressing Loss and Damage in Coastal Zones* Retrieved from https://unfccc.int/ttclear/misc_/StaticFiles/gnwoerk_static/2020_coastalzones/cfecc85aaa8d43d38cd0f6ceae2b61e4/2bb696550804403fa08df8a924922c2e.pdf

USGS. (2015). Coastal Change Hazards Portal. Retrieved from http:marine.usgs.govcoastalchangehazardsportal.

Uzair, M., & Jamil, N. (2020, 5-7 Nov. 2020). *Effects of Hidden Layers on the Efficiency of Neural networks.* Paper presented at the 2020 IEEE 23rd International Multitopic Conference (INMIC).

Van Rijn, L. C. (1993). *Principles of sediment transport in rivers, estuaries and coastal seas* (Vol. 1006): Aqua publications Amsterdam.

Van Rijn, L. C. (2007). Unified view of sediment transport by currents and waves. II: Suspended transport. *Journal of Hydraulic Engineering, 133*(6), 668-689.

Wang, B., Oldham, C., & Hipsey, M. R. (2016). Comparison of Machine Learning Techniques and Variables for Groundwater Dissolved Organic Nitrogen Prediction in an Urban Area. *Procedia Engineering, 154*, 1176-1184. doi:10.1016/j.proeng.2016.07.527

Wilson, K. E., Adams, P. N., Hapke, C. J., Lentz, E. E., & Brenner, O. (2015). Application of Bayesian Networks to hindcast barrier island morphodynamics. *Coastal Engineering, 102*, 30-43. doi:https://doi.org/10.1016/j.coastaleng.2015.04.006

Yang, S., & Browne, A. (2004). Neural network ensembles: combining multiple models for enhanced performance using a multistage approach. *Expert Systems, 21*(5), 279-288.

Yates, M. L., & Le Cozannet, G. (2012). Brief communication "Evaluating European Coastal Evolution using Bayesian Networks". *Nat. Hazards Earth Syst. Sci., 12*(4), 1173-1177. doi:10.5194/nhess-12-1173-2012

Ying, X. (2019). An Overview of Overfitting and its Solutions. *Journal of Physics: Conference Series, 1168*, 022022. doi:10.1088/1742-6596/1168/2/022022

Zeigler, S. L., Thieler, E. R., Gutierrez, B. T., Plant, N. G., Hines, M., Fraser, J. D., . . . Karpanty, S. M. (2017). Smartphone technologies and Bayesian networks to assess shorebird habitat selection. *Wildlife Society Bulletin, 41*(4), 666-677. doi:https://doi.org/10.1002/wsb.820